ORIGINAL RESEARCH

Head-to-head comparison of relative cerebral blood flow derived from dynamic [18F]florbetapir and [18F]flortaucipir PET in subjects with subjective cognitive decline

Hayel Tuncel[1], Denise Visser[1], Tessa Timmers[1,2], Emma E. Wolters[1,2], Rik Ossenkoppele[2,3], Wiesje M. van der Flier[2,4], Bart N. M. van Berckel[1], Ronald Boellaard[1] and Sandeep S. V. Golla[1*]

Abstract

Background Dynamic PET imaging studies provide accurate estimates of specific binding, but also measure the relative tracer delivery (R_1), which is a proxy for relative cerebral blood flow (rCBF). Recently, studies suggested that R_1 obtained from different tracers could be used interchangeably and is irrespective of target tissue. However, the similarities or differences of R_1 obtained from different PET tracers still require validation. Therefore, the goal of the current study was to compare R_1 estimates, derived from dynamic [18F]florbetapir (amyloid) and [18F]flortaucipir (tau) PET, in the same subjects with subjective cognitive decline (SCD).

Results Voxel-wise analysis presented a small cluster (1.6% of the whole brain) with higher R_1 values for [18F]flortaucipir compared to [18F]florbetapir in the Aβ-negative group. These voxels were part of the hippocampus and the left middle occipital gyrus. In part of the thalamus, midbrain and cerebellum, voxels (2.5% of the whole brain) with higher R_1 values for [18F]florbetapir were observed. In the Aβ-positive group, a cluster (0.2% of the whole brain) of higher R_1 values was observed in part of the hippocampus, right parahippocampal gyrus and in the left sagittal stratum for [18F]flortaucipir compared to [18F]florbetapir. Furthermore, in part of the thalamus, left amygdala, midbrain and right parahippocampal gyrus voxels (0.4% of the whole brain) with higher R_1 values for [18F]florbetapir were observed. Despite these differences, [18F]florbetapir R_1 had high correspondence with [18F]flortaucipir R_1 across all regions of interest (ROIs) and subjects (Aβ−: $r^2 = 0.79$, slope = 0.85, ICC = 0.76; Aβ+: $r^2 = 0.87$, slope = 0.93, ICC = 0.77).

Conclusion [18F]flortaucipir and [18F]florbetapir showed similar R_1 estimates in cortical regions. This finding, put together with previous studies, indicates that R_1 could be considered a surrogate for relative cerebral blood flow (rCBF) in the cortex and may be used interchangeably, but with caution, regardless of the choice of these two tracers.

Keywords PET, Relative cerebral blood flow, [18F]florbetapir, [18F]flortaucipir, SCD

*Correspondence:
Sandeep S. V. Golla
s.golla@amsterdamumc.nl
Full list of author information is available at the end of the article

Tuncel *et al. EJNMMI Research*   (2023) 13:93

Page 2 of 11

Introduction

Alzheimer's disease (AD) is a progressive neurodegenerative disorder characterized by accumulation of intracellular neurofibrillary tangles (NFTs) and extracellular amyloid-β (Aβ) plaques in the brain [1]. The accumulation causes neuropathological changes, such as synaptic and neuronal cell death and decreased cognitive function. Aβ plaques are believed to be one of the hallmarks driving AD pathogenesis and are used for diagnosis; however, there is evidence that vascular and metabolic factors are involved in the development and progression of AD as well [2]. Previous imaging studies have shown that reduced cerebral blood (CBF) and cerebral metabolic rates of glucose in the brain could serve as possible biomarkers of AD [3, 4]. More importantly, these biomarkers are associated with cognitive decline and conversion to AD; therefore, they can be used to identify clinical drug trial participants who are in a milder and earlier phase of the disease [5, 6].

Radiolabelled water, also called $[^{15}O]H_2O$, has a linear relationship with CBF [7]. Hence, the gold standard for measurement of CBF is $[^{15}O]H_2O$ positron emission tomography (PET). However, the short half-life of ^{15}O makes it difficult to use it in clinical practice. Moreover, the test–retest repeatability (TRT) of K_1 obtained for $[^{15}O]H_2O$ is quite low (9.7 ± 10.4%) [8], which is inconvenient for longitudinal or drug intervention studies. A way to measure CBF is arterial spin labelling of magnetic resonance imaging (MRI) [9] which has a good correspondence with $[^{15}O]H_2O$ PET, but also moderate reliability over time (ICC = 0.63–0.74) [10, 11]. However, previous studies have presented R_1 obtained from a dynamic PET scan as a surrogate of relative cerebral blood flow (rCBF) [12–17]. R_1 represents the ratio of tracer influx in target regions relative to the reference region and can be obtained from the same PET (dynamic) scan without requirement of any additional scans. Several studies have shown that R_1 estimates obtained with some amyloid and tau tracers such as $[^{11}C]PIB$, $[^{18}F]$THK5317 and $[^{18}F]AV45$ are strongly correlated with CBF obtained from $[^{15}O]H_2O$ PET and metabolic activity derived from $[^{18}F]FDG$ PET [12, 13, 16, 17]. Furthermore, the TRT of $[^{18}F]$florbetapir and $[^{18}F]$flortaucipir R_1 is higher when compared to the TRT of $[^{15}O]H_2O$, 2.1 ± 1.1% and 1.8 ± 1.3%, respectively [8, 18]. This suggests that dynamic $[^{18}F]$florbetapir and $[^{18}F]$flortaucipir PET scans do not only provide quantitative information of amyloid-β and tau pathology but also yield estimates on rCBF and ultimately circumvent the need for an additional $[^{15}O]H_2O$, $[^{18}F]FDG$ scan or MRI for AD patients. This approach would be highly useful in the clinic, since it results in decreased costs, lower radiation dose and increased patient comfort.

A study by Rodriguez-Vieitez [13] investigated the comparability of $[^{18}F]$THK5317- and $[^{11}C]PIB$-derived rCBF in 11 mild cognitive impairment subjects and 8 AD patients. The researchers showed a high correlation ($r = 0.90$) in R_1 between the two tracers. Moreover, another recent study found [19] a strong correlation between $[^{18}F]MK6240$ and $[^{11}C]PiB$ R_1 ($r = 0.93$). These findings suggest that R_1 obtained from different tracers could be used interchangeably and is irrespective of target tissue. Although a few studies have indicated that R_1 can be used as a surrogate of rCBF, the similarities or differences of R_1 estimates obtained from different PET tracers still require validation. It is of importance to determine whether the outcome of R_1 is similar between different tracers, since rCBF should not depend on the choice of the tracer. Therefore, the aim of the current study was to compare the R_1 estimates derived from dynamic $[^{18}F]$florbetapir and $[^{18}F]$flortaucipir PET scans and assess whether R_1 can serve as a tracer-independent surrogate of rCBF, in case of these specific tracers. To this end, a head-to-head comparison was made using $[^{18}F]$florbetapir and $[^{18}F]$flortaucipir PET scans obtained from the same subjects with subjective cognitive decline (SCD).

Methods

Participants

Fifty SCD subjects from the Amsterdam Dementia Cohort [20, 21] and Subjective Cognitive ImpairmENt Cohort (SCIENCe) study [22] were included. A standardized dementia screening was performed for all subjects, including medical history, extensive neuropsychological assessment, physical and neurological examination, lumbar puncture, blood tests, electroencephalography and brain MRI. The subjects were labelled as SCD, based on self-reported cognitive complaints, without objective impairment on neuropsychological or neurological tasks or brain damage as visualized by MRI [23]. Nineteen out of 50 SCD subjects were classified as amyloid positive as evidenced by substantial Aß pathology after visual assessment of $[^{18}F]$florbetapir Aß-PET ($SUVr_{50-70\ min}$) scans (with grey matter (GM) cerebellum as the reference region) by an experienced nuclear medicine physician. Exclusion criteria were: significant cerebrovascular disease as assessed by MRI, major traumatic brain injury, major psychiatric or neurological disorders (other than AD) and recent substance abuse. The study was approved by the Medical Ethics Review Committee of Amsterdam UMC. All subjects signed written informed consent prior to study participation. All procedures performed were in accordance with the ethical standards of the institutional research committee and with the 1975 Helsinki Declaration and its later amendments.

Tuncel *et al. EJNMMI Research*   (2023) 13:93

Page 3 of 11

Data acquisition and processing

All subjects underwent a dynamic [18F]florbetapir and [18F]flortaucipir PET scan, both acquired on a Philips Ingenuity TF-64 PET/CT scanner, with a time period of 50.6 ± 34.7 days between both PET scans. The scan procedure for the [18F]florbetapir PET scans was as followed: first, following a low-dose computed tomography (CT) scan for attenuation corrections, a 90-min dynamic PET scan was obtained with 319 ± 25 MBq [18F]florbetapir injected activity. [18F]florbetapir PET scans were reconstructed using ordered subsets time of flight (BLOB-OS-TF) into a total of 22 frames (1×15, 3×5, 3×10, 4×60, 2×150, 2×300 and 7×600 s). The scan procedure for the [18F]flortaucipir PET scans consisted of two time windows of 60 and 50 min, respectively, with a 20-min break in between. Each time window was preceded by a low-dose CT for attenuation correction. The first time window of the PET scan was acquired simultaneously with a bolus injection 241 ± 11 MBq [18F]flortaucipir. Using VINCI software (Max Plank Institute, Cologne, Germany), the second time window of the PET scan was co-registered to the first time window. The PET list mode data were rebinned into a total of 29 frames (1×15, 3×5, 3×10, 4×60, 2×150, 2×300, 4×600 and 10×300 s), and raw data were reconstructed using 3D RAMLA. During the reconstruction of all PET scans, corrections for decay, dead time, normalization, attenuation, random coincidences and scatter were applied. All reconstructed PET images, for both tracers, had a matrix size of $128 \times 128 \times 90$ and a voxel size of $2 \times 2 \times 2$ mm^3.

Furthermore, T1-weighted MRI scans were acquired for all subjects using a 3.0 T Philips Ingenuity Time-of-Flight PET/MR scanner (Philips medical systems, Best, the Netherlands) for structural information and brain tissue segmentation.

Data analysis

The T1-weighted MRI scans were co-registered onto the corresponding PET images in Vinci software. Using PVElab [24] and Hammers template [25], volumes of interest were delineated on the co-registered MR images and superimposed on the PET scan to obtain regional time activity curves (TACs). PVElab utilizes a region of interest probability map created on the basis of a database of several subjects' T1-weighted MR images, where regions of interest (ROIs) have been pre-defined manually. The PET scan and the T1-weighted MRI scan (co-registered to PET) were used as input in PVElab for each subject separately. Within PVElab, these different T1-weighted MRI scans and associated pre-segmented templates are co-registered onto the MRI scan of interest. By this, a probability map of ROIs

for the MRI scan of interest is obtained. Voxel-wise parametric images of R_1 were generated using receptor parametric mapping (RPM, a basis function approach of simplified reference tissue model) with cerebellar GM as the reference region [26–28]. For this purpose, the entire duration of the PET scan was used. For regional analysis (in subject space), the following GM bilateral ROIs were produced a priori combining brain regions from the Hammers template [25]: frontal cortex, parietal cortex, temporal cortex, occipital cortex, thalamus, putamen, hippocampus, insula, brainstem and whole brain.

Voxel-wise analyses were performed to create average images of the subject groups with different amyloid status (Aβ negative and Aβ positive) and to explore differences in [18F]florbetapir and [18F]flortaucipir R_1. For this purpose, Statistical Parametric Mapping (SPM) version 12 software (Welcome Trust Center for Neuroimaging, University College London, UK) was used. First, all native space parametric R_1 images were warped to Montreal Neurological Institute (MNI152) space using the transformation matrixes derived from warping the co-registered MRI scans to MNI space. Warped images underwent quality control in order to avoid transformation errors. After warping, PET images were smoothed by a Gaussian filter of 8 mm FWHM over a 3D space to increase signal-to-noise ratio for statistical analysis.

Statistical analyses

Paired samples t-tests were used for all the analyses (regional and voxel-wise) to compare R_1 values from [18F]florbetapir and [18F]flortaucipir scans. A *p*-value below 0.001 (uncorrected for family-wise error (FWE), with cluster size > 25 voxels) was considered significant for voxel-wise analyses. Furthermore, a more conservative FWE rate Bonferroni correction ($p < 0.05$) was assessed. In addition to the voxel-wise analysis in SPM, an additional regional analysis was performed. For that, the output of the voxel-wise SPM analysis was used to obtain a mask. In this mask, all the significantly different voxels between the two tracers from the SPM analysis had a value of one and the rest of the voxels had a value of zero, so a binary mask was obtained. This mask was used to obtain the regional R_1 values (i.e. a region for "significant voxels" and another for the "non-significant voxels") for each subject and tracer. This entire procedure was performed in MNI space. Lastly, correlations coefficients (r^2) were determined and an intraclass correlation coefficient (ICC) was calculated using an absolute agreement, two-way mixed-effects model for R_1.

Tuncel *et al. EJNMMI Research*   (2023) 13:93

Page 4 of 11

Results

The current data did now show significant differences in age ($p=0.053$) or MMSE ($p=0.40$) between the Aβ-positive and Aβ-negative subject groups. Furthermore, no significant differences were observed in R_1 between the Aβ-positive and Aβ-negative subjects in whole brain for [^{18}F]flortaucipir ($p=0.15$) and [^{18}F]florbetapir ($p=0.51$).

Comparison of average R_1 maps per tracer and amyloid status

No visual differences in the cortical regions between the average R_1 images of [^{18}F]florbetapir and [^{18}F]flortaucipir were observed, irrespective of amyloid status (Fig. 1).

Voxel-wise comparison of [^{18}F]florbetapir and [^{18}F]flortaucipir R_1 images

Aβ-negative group

Voxel-wise analysis showed higher R_1 values for [^{18}F]florbetapir when compared to [^{18}F]flortaucipir in a few clusters (2.5% of the whole brain) which were located in part of the thalamus (bilateral), midbrain (bilateral), left red nucleus, left entorhinal cortex, right hippocampus, left posterior insula, left hypothalamus, right fusiform gyrus, right nucleus accumbens, right medial temporal gyrus and small part of the cerebellum (bilateral) (Fig. 2a). Differences in these regions survived FWE correction. Furthermore, a few clusters (1.6% of the whole brain) showed higher R_1 values in the hippocampus (bilateral) and the left middle occipital gyrus for [^{18}F]flortaucipir compared to [^{18}F]florbetapir (Fig. 2b). Differences in these areas too survived FWE correction.

Aβ-positive group

Voxel-wise analysis showed small significant clusters (0.4% of the whole brain), indicating higher R_1 values for [^{18}F]florbetapir when compared to [^{18}F]flortaucipir. These clusters were mainly located in part of the thalamus (bilateral), left amygdala, midbrain (bilateral) and right parahippocampal gyrus (Fig. 2c). Even with FWE correction, these regions retained the significant differences. Furthermore, a very small cluster of significant voxels (0.2% of the whole brain) was observed for [^{18}F]flortaucipir in the hippocampus (bilateral), right parahippocampal gyrus and in the left sagittal stratum (Fig. 2d). Differences in the hippocampus and stratum survived FWE correction.
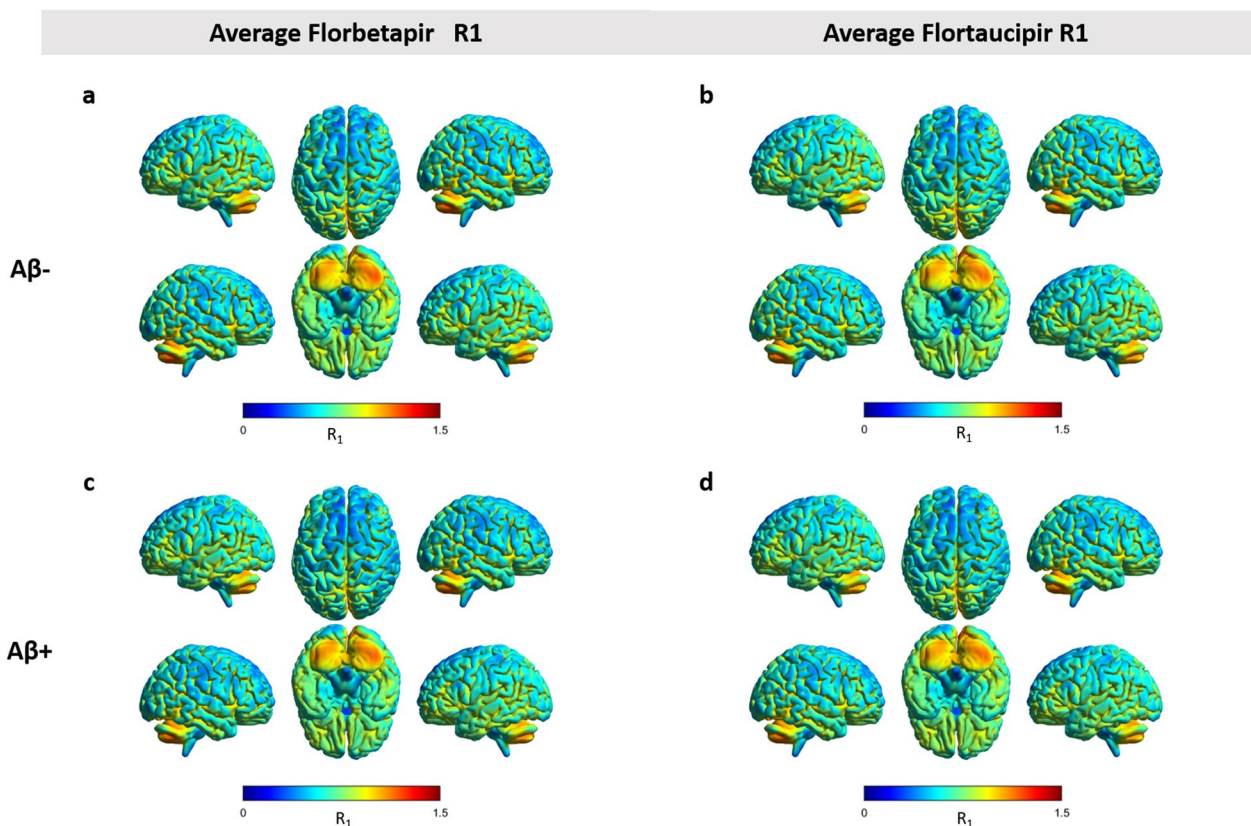

Fig. 1 Average [^{18}F]florbetapir and [^{18}F]flortaucipir R_1 images for all Aβ-negative (**a, b**) and Aβ-positive subjects (**c, d**)
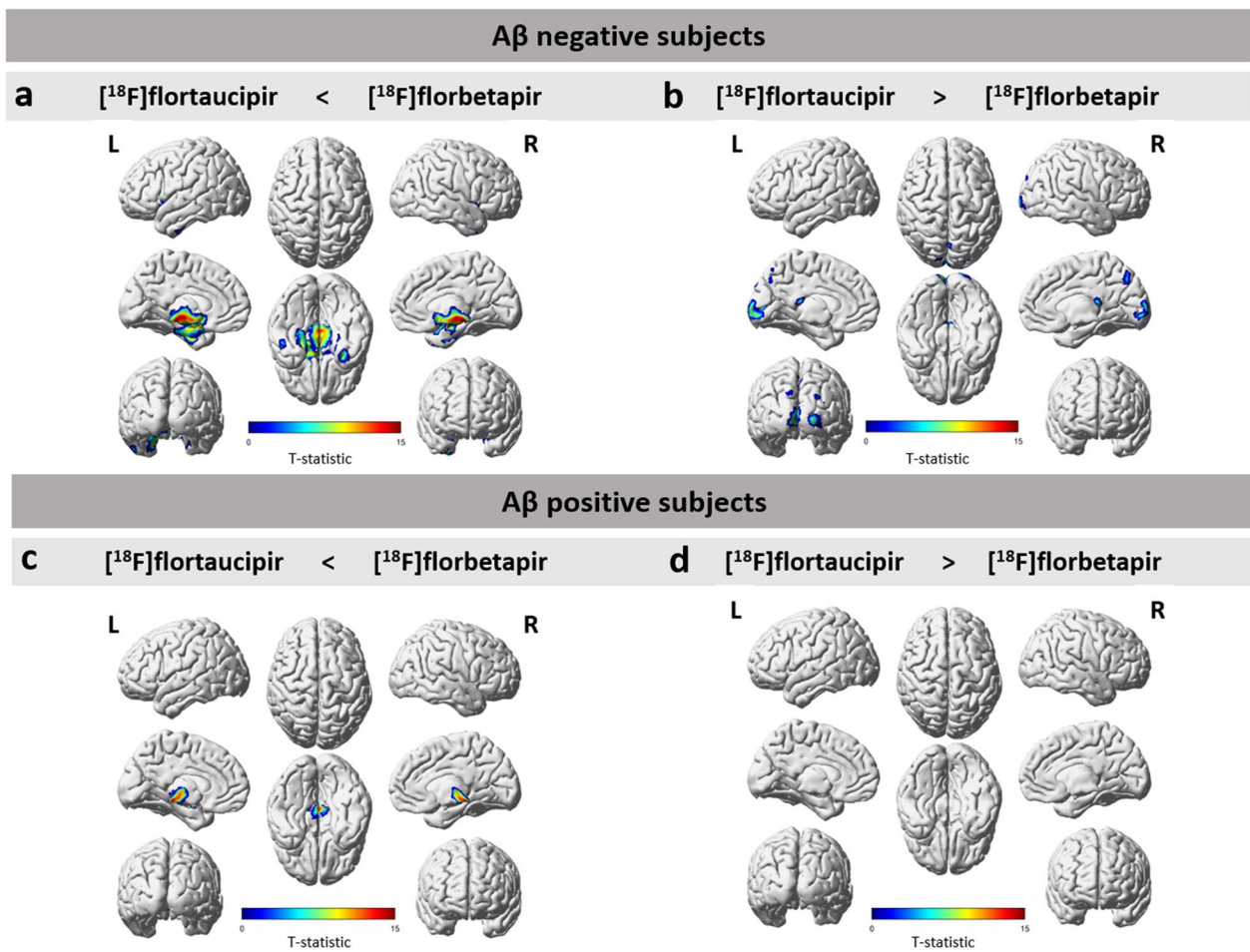
Fig. 2 Results from voxel-wise analysis using SPM12 between R_1 images of [^{18}F]flortaucipir and [^{18}F]florbetapir, separately for the Aβ-negative (**a, b**) and Aβ-positive group (**c, d**)

Difference images

Average parametric RPM R_1 difference images between [^{18}F]flortaucipir and [^{18}F]florbetapir are presented in Fig. 3, separately for Aβ-negative and Aβ-positive subjects.

Regional comparisons between [^{18}F]florbetapir and [^{18}F]flortaucipir R_1 images in MNI space

For the voxels with no significant differences in R_1 between the [^{18}F]florbetapir and [^{18}F]flortaucipir tracers, a good correspondence was observed irrespective of the amyloid status as illustrated in Fig. 4 (range r^2: 0.73–0.75, slope: 0.83–1.06). Interestingly, even for the voxels with significant differences, a good correspondence (range r^2: 0.46–0.82, slope: 0.62–0.93) was observed (Fig. 4). However, in this scenario, amyloid status seems to have a negative impact on the correspondence.

Regional [^{18}F]florbetapir and [^{18}F]flortaucipir R1 comparisons in native space

The Aβ-negative group showed significant differences in the parietal cortex, temporal cortex, occipital cortex, hippocampus, thalamus and insula (Fig. 5). Furthermore, significant differences were found in the occipital cortex, thalamus and insula in the Aβ-positive group (Fig. 5). Despite that the R_1 for some regions was significantly different between the tracers, most of the regions had a good to moderate correlation for R_1 obtained with [^{18}F]florbetapir and [^{18}F]flortaucipir (Fig. 6). Also for the Aβ-positive group, most of the regions had a good to moderate correlation for R_1 obtained with [^{18}F]florbetapir and [^{18}F]flortaucipir (Fig. 6).

The ICC for each brain region (in native space) is presented in Table 1, separately for the Aβ-negative and Aβ-positive subjects. Most of the regions had an excellent ICC > 0.80; however, the smaller regions had somewhat lower ICC < 0.70.
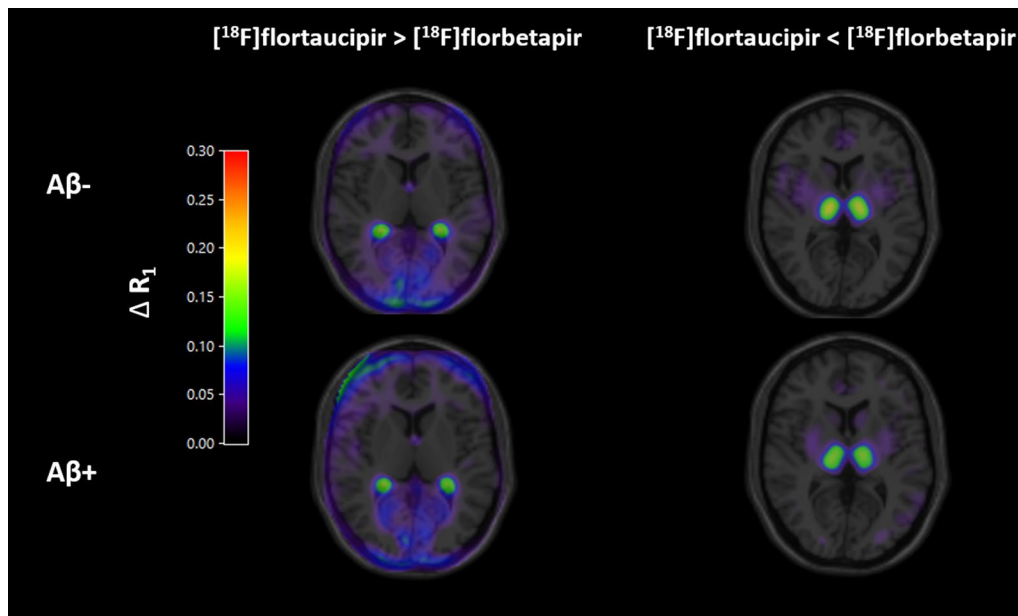
Fig. 3 Average ΔR_1 images superimposed with T1-weighted MRI scan in MNI space: average of the ΔR_1 images in MNI space for different conditions ([^{18}F]flortaucipir > [^{18}F]florbetapir and, [^{18}F]flortaucipir < [^{18}F]florbetapir) separately for Aβ-negative and Aβ-positive subjects are illustrated

Discussion

The current study made a head-to-head comparison between R_1 obtained from two different dynamic PET tracers. In line with previous studies [13, 19], the results of the current study showed that RPM R_1 derived from dynamic [^{18}F]florbetapir and [^{18}F]flortaucipir PET scans were well correlated with each other irrespective of the small clusters (range 0.2–2.6% of the whole brain) with significant differences observed during voxel-wise comparisons. In a previous head-to-head comparison study, it has been demonstrated that R_1 estimates from a [^{18}F]florbetapir PET scan strongly correlated with CBF obtained from [^{15}O]H$_2$O PET [17]. Based on the results of the current study and the study by Ottoy et al. (2019) [17], one could state that R_1 may serve as a surrogate for rCBF, for both [^{18}F]flortaucipir and [^{18}F]florbetapir (particularly for cortical regions). The R_1 obtained with [^{18}F]florbetapir and [^{18}F]flortaucipir PET are of clinical interest as amyloid and tau tracers benefit from the ability to provide information on both rCBF and Aβ pathology or tau pathology in one imaging session, respectively. Most of the cortical regions had no significant differences in R_1 between the tracers for both Aβ-negative and Aβ-positive SCD subjects. Despite the significant clusters, the R_1 obtained from [^{18}F]florbetapir and [^{18}F]flortaucipir were well correlated ($r^2 > 0.5$). These findings were supported by the results of the regional analysis in native space.

Significantly higher R_1 values in the hippocampus for [^{18}F]flortaucipir were observed when compared to [^{18}F]florbetapir in both Aβ-negative and Aβ-positive SCD subjects. Hippocampus is a region that is crucial in AD with respect to tau studies, since the involvement of the hippocampus is thought to occur at a critical stage of tau pathology progression [29]. [^{18}F]flortaucipir has been characterized by off-target binding in the basal ganglia, thalamus and choroid plexus [30–32]. The off-target binding in the choroid plexus is of particular interest since it may cause spill-in to the anatomically near hippocampus. This spill-in effect may lead to an artificially increased [^{18}F]flortaucipir activity in the hippocampus which leads to an inaccurate quantification of hippocampal tau load. The choroid plexus consists of a dense collection of capillaries in an ependymal stroma surrounded by a layer of epithelium [33]. The choroid plexus of the lateral ventricles may have several structures that could bind to [^{18}F]flortaucipir, including melanin [34], calcification [35], Biondi bodies [36, 37] and iron deposits [38]. Off-target binding is problematic as the hippocampus is among the earliest regions affected by tau pathology and accurate assessment of tau accumulation in this region is important in the understanding of the natural time course of AD [29]. Earlier studies have investigated methods to reduce the spill-in effect of the choroid plexus, such as eroding voxels of the hippocampus [39], various partial volume correction methods [39–41] and linear regression approaches [39, 40]. These techniques led to decreased correlation between hippocampus and choroid plexus tracer binding, presumably due to decreasing
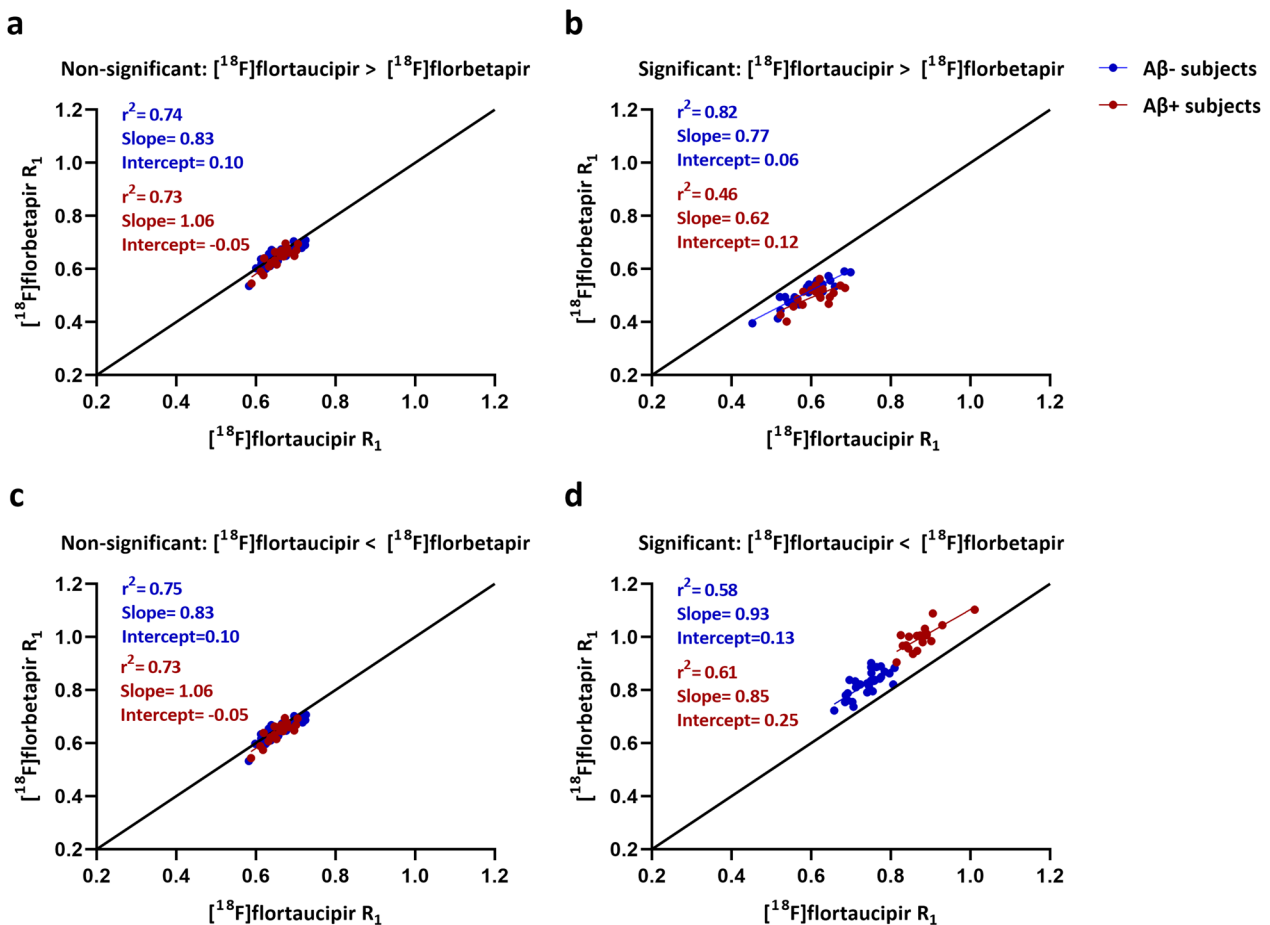
Tuncel *et al. EJNMMI Research*   (2023) 13:93

Page 7 of 11

Fig. 4 Correlations and slopes between [18F]flortaucipir R_1 and [18F]florbetapir R_1 for significant (**b, d**) and non-significant voxels (**a, c**). Two conditions are also illustrated in the figure: [18F]flortaucipir > [18F]florbetapir (**a, b**) and [18F]flortaucipir < [18F]florbetapir (**c, d**). Each dot in the figure represents a subject (blue dots represent amyloid-negative subjects and red dots represent amyloid-positive subjects). Significant: Voxels with significant differences from the voxel-wise analysis. Non-significant: Voxels with no significant differences from the voxel-wise analysis

the spill-in effects [39–42]. The elevated [18F]flortaucipir signal in the hippocampus when compared to [18F]florbetapir could be partly explained by spill-in from the off-target binding in the choroid plexus.

Higher R_1 values were observed for [18F]florbetapir in part of the thalamus (bilateral) when compared to [18F]flortaucipir in both Aβ-negative and Aβ-positive SCD subjects. The thalamus mainly consists of GM; however, it also contains two thin layers of white matter (WM), including the stratum zonale that covers the dorsal surface, and the external and internal medullary laminae [43]. [18F]florbetapir has previously shown non-specific binding in WM [44]. WM mainly consists of myelin, which is highly lipidic. The lipophilic character of [18F]florbetapir presumably explains the non-specific binding in this region [45, 46]. In our study, the number of voxels that were significant in the thalamus for WM was ± 863 voxels for Aβ-negative SCD subjects, accounting for 55.4% of total voxels in the WM thalamus and ± 500

voxels (31.5% of total voxels in the WM thalamus) for Aβ-positive SCD subjects, while the significant number of voxels in the GM for this region was much lower (Aβ−: ± 211 voxels: 24.1% of total GM voxels, Aβ+: ± 155 voxels; 17.7% of total GM voxels). This may be a possible explanation for the observed significant differences in R_1 between [18F]florbetapir and [18F]flortaucipir in the thalamus in this study.

A decrease in rCBF in the thalamus in case of Aβ-positive SCD subjects (as shown in Fig. 6, subplot associated with Thalamus) could be because of the involvement of the Papez circuit in the memory function. The Papez circuit is an anatomical circuit which starts and ends in the hippocampus [47]. Earlier studies have shown that lesions in any part of this circuit can cause memory dysfunction [48–50]. It is not uncommon that there is decreased cerebral blood flow in the thalamus in Aβ-positive SCD subjects [51]. Kobayashi et al. [51] also observed decreased thalamic blood flow in mild AD
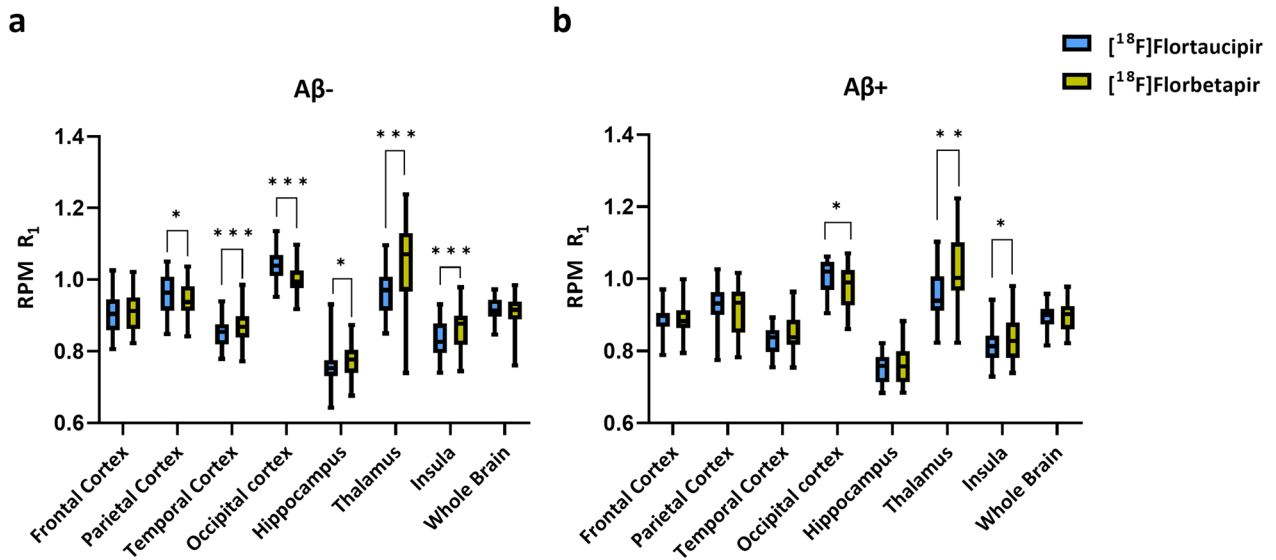
Fig. 5 Bar plots illustrating the regional comparisons of R_1 values (in native space) of [^{18}F]flortaucipir and [^{18}F]florbetapir, separately for Aβ-negative (**a**) and Aβ-positive (**b**) subjects
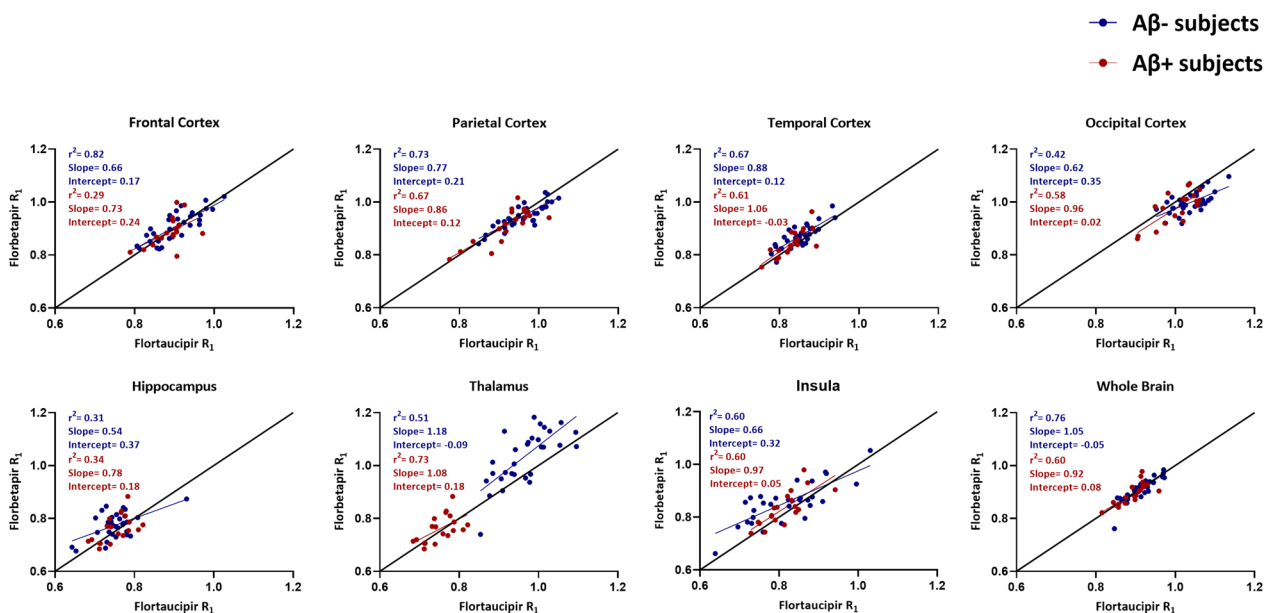

Fig. 6 Correlations and slopes obtained from the regional analysis (in native space) between [^{18}F]flortaucipir R_1 and [^{18}F]florbetapir R_1 for Aβ-negative and Aβ-positive subjects

patients using quantitative brain perfusion SPECT. The researchers concluded that lower rCBF in the thalamus might be the result of a remote metabolic effect in the Papez circuit.

Almost all other GM cortical regions showed similar R_1 values for both tracers. Besides that, the R_1 values obtained from [^{18}F]flortaucipir and [^{18}F]florbetapir showed good correspondence in the voxel-wise analysis

and in the regional analysis (Figs. 4, 6), indicating that R_1 may be considered as a reliable measure of cortical rCBF irrespective of tracer choice. The smaller brain regions, such as the insula and hippocampus, had weaker correlations in R_1 between the two tracers, and this could be explained by the fact that smaller regions are more prone to noise. Furthermore, some ROIs showed significant differences in the Aβ-negative subjects that were not present

Tuncel *et al. EJNMMI Research*   (2023) 13:93

Page 9 of 11

Table 1 ICC between regional [18F]flortaucipir R_1 and [18F]florbetapir R_1 (in native space), separately for Aβ-negative and Aβ-positive subjects

	ICC	
	Aβ negative	Aβ positive
Frontal cortex	0.90	0.70
Parietal cortex	0.91	0.90
Temporal cortex	0.85	0.83
Occipital cortex	0.62	0.81
Hippocampus	0.67	0.72
Thalamus	0.66	0.81
Insula	0.84	0.84
Putamen	0.65	0.85
Brainstem	0.61	0.32
Whole brain	0.92	0.87

in the Aβ-positive group. No clarification could be found for these results. Therefore, further research, aimed to address this issue, is necessary to determine the clinical implications. Despite different kinetics, the present study showed that R_1 obtained from [18F]florbetapir was comparable with [18F]flortaucipir R_1 in the cortical regions. Furthermore, the TRT of R_1 is better for both tracers, $2.1 \pm 1.1\%$ and $1.8 \pm 1.3\%$ [8, 18], respectively, when compared to the TRT of perfusion as measured with [15O] H_2O PET ($9.7 \pm 10.4\%$) [8]. K_1 estimates obtained from [15O]H_2O PET presented a lower test–retest repeatability, possibly due to day to day intrasubject variabilities (that are not related to any underlying pathology). Since the intrasubject differences (non-pathological) remain more or less constant throughout the brain, normalizing the K_1 to a reference region K_1' (i.e. R_1) could correct for these differences and improve the TRT.

One of the limitations of the current study is that it was performed only in SCD subjects. It should preferably be reevaluated in patient groups, especially if pathological alterations in rCBF are expected such as in neurodegenerative disorders. For this purpose, the gold standard, [15O]H_2O PET can be considered to evaluate direct CBF in first place. Furthermore, no partial volume correction method was applied on the data, which can eliminate the spill-in effects from the choroid plexus and the WM. Yet, as both tracer studies were collected on the same PET system and used the same reconstruction methods and settings, both datasets have a matched spatial resolution. It is important to acknowledge that partial volume effects (PVE) depend on the contrast between regions, influenced by both tracer and uptake time. Consequently, PVE may not be the same across the tracers under examination. However, R_1 is primarily determined by the early uptake phase of the tracer (< 100 s). Therefore, we anticipate that the influence of PVE on R_1 may be similar for both tracers. Nonetheless, certain distinctions, such as possible spill-in from the choroid plexus and white matter, cannot be definitively dismissed. Additionally, validation of the use of R_1 as cortical rCBF surrogate was evaluated for [18F]florbetapir and [18F]flortaucipir and it is essential to note that the extension of these results to other tracers requires further assessments.

Conclusion

The present study showed that [18F]flortaucipir and [18F]florbetapir R_1 values were well correlated in GM cortical regions. Put together with previous findings by Ottoy et al. (2019) [17], a cautious claim can be made that R_1 values of both tracers are a valid marker for cortical rCBF. However, the use of R_1 as a tracer-independent rCBF surrogate should be performed with caution in case of some non-cortical areas, as shown in this study. Furthermore, generalization to other tracers is not directly implied by this study, since each new PET tracer needs thorough validation.

Abbreviations

Aβ	Amyloid beta
AD	Azheimer's disease
CBF	Cerebral blood flow
FDG	[18F]-fluoro-2-deoxy-D-glucose
FWE	Family-wise error
ICC	Intraclass correlation coefficient
MNI	Montreal Neurological Institute
MRI	Magnetic resonance imaging
PET	Positron emission tomography
r^2	Correlation coefficient
rCBF	Relative cerebral blood flow
ROIs	Regions of interest
RPM	Receptor parametric mapping
SCD	Subjective cognitive decline
SPM12	Statistical Parametric Mapping 12
SRTM	Simplified reference tissue model
SUVr	Standardized uptake value ratio
TAC	Time activity curve
TRT	Test–retest repeatability

Author contributions

HT, SG, BB and RB contributed to the concept and design of the study. EW, TT and DV acquired the data. HT, SG, MY and RB contributed to the analysis and interpretation of the data. HT drafted the manuscript. HT, SG, EW, TT, DV, WF, RO, BB and RB read, critically reviewed and approved the manuscript.

Availability of data and materials

The datasets used and/or analysed during the current study are available from the corresponding author on reasonable request.

Declarations

Ethics approval and consent to participate

The current study was approved by the Medical Ethics Committee of the Amsterdam University Medical Center. All subjects signed an informed consent form prior to participation. All procedures performed were in accordance with the ethical standards of the institutional research committee and with the 1975 Helsinki Declaration and its later amendments.

Consent for publication

Not applicable.

Competing interests

No potential competing of interest relevant to this article exists.

Author details

[1]Department of Radiology and Nuclear Medicine, Amsterdam Neuroscience, Vrije Universiteit Amsterdam, Amsterdam UMC, De Boelelaan 1117, 1081 HV Amsterdam, The Netherlands. [2]Department of Neurology, Alzheimer Center Amsterdam, Vrije Universiteit Amsterdam, Amsterdam UMC, Amsterdam, The Netherlands. [3]Clinical Memory Research Unit, Lund University, Lund, Sweden. [4]Department of Epidemiology and Biostatistics, Vrije Universiteit Amsterdam, Amsterdam UMC, Amsterdam, The Netherlands.

References

1. Holtzman DM, Morris JC, Goate AM. Alzheimer's disease: the challenge of the second century. Sci Transl Med. 2011;3(77):77sr1.
2. Rius-Pérez S, Tormos AM, Pérez S, Taléns-Visconti R. Vascular pathology: Cause or effect in Alzheimer disease? Neurologia (Engl Ed). 2018;33(2):112–20.
3. Binnewijzend MA, Benedictus MR, Kuijer JP, van der Flier WM, Teunissen CE, Prins ND, et al. Cerebral perfusion in the predementia stages of Alzheimer's disease. Eur Radiol. 2016;26(2):506–14.
4. Mosconi L, Berti V, Glodzik L, Pupi A, De Santi S, de Leon MJ. Pre-clinical detection of Alzheimer's disease using FDG-PET, with or without amyloid imaging. J Alzheimers Dis. 2010;20(3):843–54.
5. Hirao K, Ohnishi T, Hirata Y, Yamashita F, Mori T, Moriguchi Y, et al. The prediction of rapid conversion to Alzheimer's disease in mild cognitive impairment using regional cerebral blood flow SPECT. Neuroimage. 2005;28(4):1014–21.
6. Benedictus MR, Leeuwis AE, Binnewijzend MA, Kuijer JP, Scheltens P, Barkhof F, et al. Lower cerebral blood flow is associated with faster cognitive decline in Alzheimer's disease. Eur Radiol. 2017;27(3):1169–75.
7. Herscovitch P, Markham J, Raichle ME. Brain blood flow measured with intravenous H2(15)O. I. Theory and error analysis. J Nucl Med. 1983;24(9):782–9.
8. Heeman F, Visser D, Yaqub M, Verfaillie S, Timmers T, Pijnenburg YA, et al. Precision estimates of relative and absolute cerebral blood flow in Alzheimer's disease and cognitively normal individuals. J Cereb Blood Flow Metab. 2023;43(3):369–78.
9. Zhang N, Gordon ML, Goldberg TE. Cerebral blood flow measured by arterial spin labeling MRI at resting state in normal aging and Alzheimer's disease. Neurosci Biobehav Rev. 2017;72:168–75.
10. Xu G, Rowley HA, Wu G, Alsop DC, Shankaranarayanan A, Dowling M, et al. Reliability and precision of pseudo-continuous arterial spin labeling perfusion MRI on 3.0 T and comparison with 15O-water PET in elderly subjects at risk for Alzheimer's disease. NMR Biomed. 2010;23(3):286–93.
11. Jiang L, Kim M, Chodkowski B, Donahue MJ, Pekar JJ, Van Zijl PC, Albert M. Reliability and reproducibility of perfusion MRI in cognitively normal subjects. Magn Reson Imaging. 2010;28(9):1283–9.
12. Peretti DE, Vállez García D, Reesink FE, van der Goot T, De Deyn PP, de Jong BM, et al. Relative cerebral flow from dynamic PIB scans as an alternative for FDG scans in Alzheimer's disease PET studies. PLoS ONE. 2019;14(1):e0211000.
13. Rodriguez-Vieitez E, Leuzy A, Chiotis K, Saint-Aubert L, Wall A, Nordberg A. Comparability of [(18)F]THK5317 and [(11)C]PIB blood flow proxy images with [(18)F]FDG positron emission tomography in Alzheimer's disease. J Cereb Blood Flow Metab. 2017;37(2):740–9.
14. Peretti DE, Vállez García D, Reesink FE, Doorduin J, de Jong BM, De Deyn PP, et al. Diagnostic performance of regional cerebral blood flow images derived from dynamic PIB scans in Alzheimer's disease. EJNMMI Res. 2019;9(1):59.
15. Joseph-Mathurin N, Su Y, Blazey TM, Jasielec M, Vlassenko A, Friedrichsen K, et al. Utility of perfusion PET measures to assess neuronal injury in Alzheimer's disease. Alzheimers Dement. 2018;10:669–77.
16. Chen YJ, Rosario BL, Mowrey W, Laymon CM, Lu X, Lopez OL, et al. Relative 11C-PiB delivery as a proxy of relative CBF: quantitative evaluation using single-session 15O-water and 11C-PiB PET. J Nucl Med. 2015;56(8):1199–205.
17. Ottoy J, Verhaeghe J, Niemantsverdriet E, De Roeck E, Wyffels L, Ceyssens S, et al. (18)F-FDG PET, the early phases and the delivery rate of (18) F-AV45 PET as proxies of cerebral blood flow in Alzheimer's disease: validation against (15)O-H(2)O PET. Alzheimers Dement. 2019;15(9):1172–82.
18. Tuncel H, Visser D, Yaqub M, Timmers T, Wolters EE, Ossenkoppele R, et al. Effect of shortening the scan duration on quantitative accuracy of [(18)F] Flortaucipir studies. Mol Imaging Biol. 2021;23(4):604–13.
19. Guehl NJ, Dhaynaut M, Hanseeuw BJ, Moon SH, Lois C, Thibault E, et al. Measurement of cerebral perfusion indices from the early phase of [(18)F] MK6240 dynamic tau PET imaging. J Nucl Med. 2023;64(6):968–75.
20. van der Flier WM, Scheltens P. Amsterdam dementia cohort: performing research to optimize care. J Alzheimers Dis. 2018;62(3):1091–111.
21. van der Flier WM, Pijnenburg YA, Prins N, Lemstra AW, Bouwman FH, Teunissen CE, et al. Optimizing patient care and research: the Amsterdam dementia cohort. J Alzheimers Dis. 2014;41(1):313–27.
22. Slot RER, Verfaillie SCJ, Overbeek JM, Timmers T, Wesselman LMP, Teunissen CE, et al. Subjective cognitive impairment cohort (SCIENCe): study design and first results. Alzheimers Res Ther. 2018;10(1):76.
23. Jessen F, Amariglio RE, van Boxtel M, Breteler M, Ceccaldi M, Chételat G, et al. A conceptual framework for research on subjective cognitive decline in preclinical Alzheimer's disease. Alzheimers Dement. 2014;10(6):844–52.
24. Svarer C, Madsen K, Hasselbalch SG, Pinborg LH, Haugbøl S, Frøkjaer VG, et al. MR-based automatic delineation of volumes of interest in human brain PET images using probability maps. Neuroimage. 2005;24(4):969–79.
25. Hammers A, Allom R, Koepp MJ, Free SL, Myers R, Lemieux L, et al. Three-dimensional maximum probability atlas of the human brain, with particular reference to the temporal lobe. Hum Brain Mapp. 2003;19(4):224–47.
26. Gunn RN, Lammertsma AA, Hume SP, Cunningham VJ. Parametric imaging of ligand-receptor binding in PET using a simplified reference region model. Neuroimage. 1997;6(4):279–87.
27. Verfaillie SC, Golla SS, Timmers T, Tuncel H, van der Weijden CW, Schober P, et al. Repeatability of parametric methods for [(18)F]florbetapir imaging in Alzheimer's disease and healthy controls: A test-retest study. J Cereb Blood Flow Metab. 2021;41(3):569–78.
28. Golla SS, Wolters EE, Timmers T, Ossenkoppele R, van der Weijden CW, Scheltens P, et al. Parametric methods for [(18)F]flortaucipir PET. J Cereb Blood Flow Metab. 2020;40(2):365–73.
29. Price JL, Morris JC. Tangles and plaques in nondemented aging and "preclinical" Alzheimer's disease. Ann Neurol. 1999;45(3):358–68.
30. Marquié M, Normandin MD, Vanderburg CR, Costantino IM, Bien EA, Rycyna LG, et al. Validating novel tau positron emission tomography tracer [F-18]-AV-1451 (T807) on postmortem brain tissue. Ann Neurol. 2015;78(5):787–800.
31. Vermeiren C, Motte P, Viot D, Mairet-Coello G, Courade JP, Citron M, et al. The tau positron-emission tomography tracer AV-1451 binds with similar affinities to tau fibrils and monoamine oxidases. Mov Disord. 2018;33(2):273–81.
32. Lowe VJ, Curran G, Fang P, Liesinger AM, Josephs KA, Parisi JE, et al. An autoradiographic evaluation of AV-1451 Tau PET in dementia. Acta Neuropathol Commun. 2016;4(1):58.

33. Wolburg H, Paulus W. Choroid plexus: biology and pathology. Acta Neuropathol. 2010;119(1):75–88.
34. Puri D. Textbook of medical biochemistry. New Delhi: Elsevier; 2006.
35. Johanson C, McMillan P, Tavares R, Spangenberger A, Duncan J, Silverberg G, Stopa E. Homeostatic capabilities of the choroid plexus epithelium in Alzheimer's disease. Cerebrospinal Fluid Res. 2004;1(1):3.
36. Miklossy J, Kraftsik R, Pillevuit O, Lepori D, Genton C, Bosman FT. Curly fiber and tangle-like inclusions in the ependyma and choroid plexus–a pathogenetic relationship with the cortical Alzheimer-type changes? J Neuropathol Exp Neurol. 1998;57(12):1202–12.
37. Wen GY, Wisniewski HM, Kascsak RJ. Biondi ring tangles in the choroid plexus of Alzheimer's disease and normal aging brains: a quantitative study. Brain Res. 1999;832(1–2):40–6.
38. Mesquita SD, Ferreira AC, Sousa JC, Santos NC, Correia-Neves M, Sousa N, et al. Modulation of iron metabolism in aging and in Alzheimer's disease: relevance of the choroid plexus. Front Cell Neurosci. 2012;6:25.
39. Wolters EE, Golla SSV, Timmers T, Ossenkoppele R, van der Weijden CWJ, Scheltens P, et al. A novel partial volume correction method for accurate quantification of [(18)F] flortaucipir in the hippocampus. EJNMMI Res. 2018;8(1):79.
40. Schöll M, Lockhart SN, Schonhaut DR, O'Neil JP, Janabi M, Ossenkoppele R, et al. PET imaging of tau deposition in the aging human brain. Neuron. 2016;89(5):971–82.
41. Wang L, Benzinger TL, Su Y, Christensen J, Friedrichsen K, Aldea P, et al. Evaluation of tau imaging in staging alzheimer disease and revealing interactions between β-amyloid and tauopathy. JAMA Neurol. 2016;73(9):1070–7.
42. Lee CM, Jacobs HIL, Marquié M, Becker JA, Andrea NV, Jin DS, et al. 18F-flortaucipir binding in choroid plexus: related to race and hippocampus signal. J Alzheimers Dis. 2018;62(4):1691–702.
43. Tortora GA, N. Principles of anatomy and physiology. 5th ed. New York: Harper & Row; 1987.
44. Wong DF, Rosenberg PB, Zhou Y, Kumar A, Raymont V, Ravert HT, et al. In vivo imaging of amyloid deposition in Alzheimer disease using the radioligand 18F-AV-45 (florbetapir [corrected] F 18). J Nucl Med. 2010;51(6):913–20.
45. Choi SR, Golding G, Zhuang Z, Zhang W, Lim N, Hefti F, et al. Preclinical properties of 18F-AV-45: a PET agent for Abeta plaques in the brain. J Nucl Med. 2009;50(11):1887–94.
46. Fleisher AS, Chen K, Liu X, Roontiva A, Thiyyagura P, Ayutyanont N, et al. Using positron emission tomography and florbetapir F18 to image cortical amyloid in patients with mild cognitive impairment or dementia due to Alzheimer disease. Arch Neurol. 2011;68(11):1404–11.
47. Papez JW. A proposed mechanism for emotion. Arch Neurol Psychiatry; 1937.
48. Sutherland RJ, Whishaw IQ, Kolb B. Contributions of cingulate cortex to two forms of spatial learning and memory. J Neurosci. 1988;8(6):1863–72.
49. Sziklas V, Petrides M. Memory impairments following lesions to the mammillary region of the rat. Eur J Neurosci. 1993;5(5):525–40.
50. Aggleton JP, Brown MW. Episodic memory, amnesia, and the hippocampal-anterior thalamic axis. Behav Brain Sci. 1999;22(3):425–44 (**discussion 44–89**).
51. Kobayashi S, Tateno M, Utsumi K, Takahashi A, Saitoh M, Morii H, et al. Quantitative analysis of brain perfusion SPECT in Alzheimer's disease using a fully automated regional cerebral blood flow quantification software, 3DSRT. J Neurol Sci. 2008;264(1–2):27–33.

Publisher's Note